Exploration for Two-Dimensional Electrides via Database Screening and *Ab Initio* Calculation

Takeshi Inoshita,[1] Sehoon Jeong,[2] Noriaki Hamada,[3] and Hideo Hosono[2]
[1]*National Institute for Materials Science, Tsukuba, Ibaraki 305-0044, Japan*
[2]*Materials and Structures Laboratory, Tokyo Institute of Technology, Nagatsuta, Kanagawa 226-8503, Japan*
[3]*Faculty of Science and Technology, Tokyo University of Science, Noda, Chiba 278-8510, Japan*
(Received 9 November 2013; revised manuscript received 10 April 2014; published 4 August 2014)

Inspired by the recent demonstration that Ca_2N is a two-dimensional electride in which electrons near the Fermi level float between ionic layers, we have conducted a systematic search for 2D electrides by an approach combining crystal structure databases and *ab initio* electronic structure calculations. Starting from a set of working hypotheses, we have identified six 2D metallic electrides, of which one is nonmagnetic and five are nearly ferromagnetic ferrimagnets with a distinct spin texture. The latter five materials are the first magnetic electrides reported at ambient pressure.

DOI: 10.1103/PhysRevX.4.031023

Subject Areas: Condensed Matter Physics, Interdisciplinary Physics, Materials Science

I. INTRODUCTION

Electrides are ionic crystals in which electrons serve as anions, occupying the space normally occupied by anions [1,2]. Since these electrons are not bound to any ions, electrides may be viewed as excess-electron materials where there is an intrinsic excess of electrons based on the formal valences of the constituent elements. Pioneered by Dye and co-workers [3], research on electrides has progressed steadily, but, until recently, all the known electrides were zero or one dimensional [4]. (Here, the dimension refers to that of the electron-confining space and therefore that of the electronic structure.) Most of these electrides are extremely sensitive to the ambient atmosphere, but the first electride that was air resistant, thermally stable, and chemically inert was synthesized by Matsuishi *et al.* [5], paving the way for the application of electrides.

In view of the overwhelming importance of two-dimensional (2D) materials in electronic devices and also in the conceptual development of condensed-matter physics and chemistry, it is natural to wonder whether there are electrides with a 2D electronic structure. Research in this direction has continued [6,7], and recently, Lee *et al.* [8] demonstrated that dicalcium nitride (Ca_2N) is a 2D electride in which conduction electrons are confined between calcium layers with a concentration in good agreement with the chemical formula $[Ca_2N]^+e^-$. The 2D nature of its electronic structure was confirmed by both transport measurements and a band calculation. Moreover, Ca_2N was found to have a very small work function (2.6–3.5 eV, depending on the surface orientation) [8], making it attractive for use as an electron emitter [9]. Shortly afterward, Walsh and Scanlon calculated the electronic structures of Sr_2N and Ba_2N and showed that they are also 2D electrides that are very similar to Ca_2N [10].

Now, the question arises as to whether there are 2D electrides other than M_2N (M = Ca, Sr, Ba). The present paper answers this question in the affirmative through a systematic screening of crystal structure databases combined with *ab initio* band calculations.

II. SCREENING CONDITIONS

Searching for a new material requires screening conditions at the starting point. We employ the following conditions, or working hypotheses. (1) The target materials are binary stoichiometric compounds M_nX_m, where M

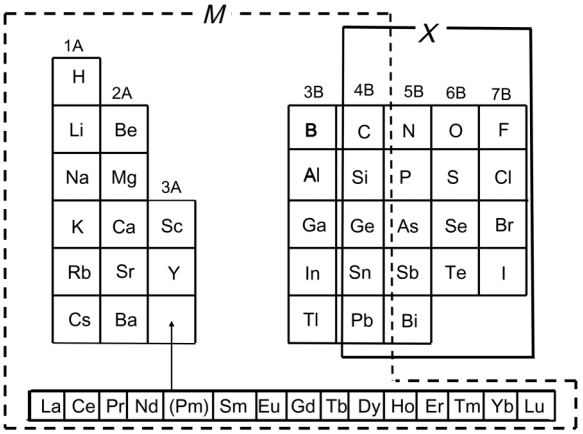

FIG. 1. Elements considered in the screening for 2D electrides.

TABLE I. Materials satisfying all the screening conditions. Here, S denotes the sum of the oxidation numbers of the constituent elements in a primitive rhombohedral unit cell (M_2X). The lattice constants (in the hexagonal setting) and magnetic moments per lanthanide ion obtained in the present calculation are compared with the experimental values. The values before and after a slash represent the values obtained with $U - J = 6$ and 9 eV (with J fixed at 0.7 eV), respectively. The magnetic moment m is obtained by dividing the total magnetization per unit cell by the number of lanthanide ions therein.

				a (Å)		c (Å)		m (μ_B)	
	S	Space group (No.)	Structure type	calculation	experiment	calculation	experiment	calculation	experiment
Ca_2N	1	$R\bar{3}m$ (166)	Anti-$CdCl_2$	3.50	3.624,[a] 3.627[b]	18.75	19.10,[a] 18.97[b]	···	···
Sr_2N	1	$R\bar{3}m$ (166)	Anti-$CdCl_2$	3.86	3.855,[c] 3.762[d]	20.95	20.725,[c] 19.589[d]	···	···
Ba_2N	1	$R\bar{3}m$ (166)	Anti-$CdCl_2$	4.05	4.029,[c] 3.991[d]	22.85	22.425,[c] 22.079[d]	···	···
Y_2C	2	$R\bar{3}m$ (166)	Anti-$CdCl_2$	3.61	3.617,[e] 3.625[f]	18.45	17.960,[e] 17.964[f]	···	···
Gd_2C	2	$R\bar{3}m$ (166)	Anti-$CdCl_2$	3.65/3.64	3.639[g]	18.50/18.43	18.415[g]	7.73/7.76	7.26[g]
Tb_2C	2	$R\bar{3}m$ (166)	Anti-$CdCl_2$	3.59/3.56	3.584,[h] 3.595[i]	18.39/18.28	18.040,[h] 18.190[i]	6.52/6.69	7.6[h]
Dy_2C	2	$R\bar{3}m$ (166)	Anti-$CdCl_2$	3.57/3.52	3.584[h]	18.35/18.20	17.890[h]	5.41/5.49	6.8[h]
Ho_2C	2	$R\bar{3}m$ (166)	Anti-$CdCl_2$	3.55/3.50	3.556,[j] 3.550[j]	18.19/18.05	17.70,[j] 17.67[j]	4.36/4.46	7.16[j]
Er_2C	2	$R\bar{3}m$ (166)	Anti-$CdCl_2$	3.56/3.55	···	18.07/18.06	···	3.27/3.28	···

[a]Reference [6].
[b]Reference [15].
[c]Reference [16].
[d]Reference [17].
[e]Reference [18].
[f]Reference [19].
[g]Reference [13].
[h]Reference [14].
[i]Reference [20].
[j]Reference [21].

(the cation) is selected from groups 1A, 2A, 3A, 3B, and 4B, and X (the anion) is selected from groups 4B to 7B of the periodic table (Fig. 1). Transition metals are excluded because they can take multiple valences. (2) The structure is layered with interlayer spacing > 3.0 Å. (3) The ions on both sides of the interlayer gap are cations. (4) The sum (S) of the oxidation numbers (O) of the constituent ions > 0.

The second condition states roughly that the cation layers are separated by a van der Waals gap. The third condition follows from the fact that the electrostatic potential in the space between cation layers (the cation-cation gap) is much deeper than inside an anion-anion gap [10], which we confirm through our calculation. Conditions (2) and (3) may be replaced by a more elaborate condition such as one based on the ionic radius and direct cation-cation distance, but our results show that the simple conditions (2) and (3) suffice. The fourth condition ensures that there are excess electrons from the viewpoint of the standard valence: For example, GaAs has $S = 0$ (no excess electron) with $O(\mathrm{Ga}) = 3$ and $O(\mathrm{As}) = -3$, while Ca_2N has $S = 1$ (one excess electron) with $O(\mathrm{Ca}) = 2$ and $O(\mathrm{N}) = -3$.

III. DATABASE SCREENING

Currently, there are two large-scale inorganic crystal structure databases in the world: MatNavi [11] and the Inorganic Crystal Structure Database (ICSD) [12]. We search both databases and identify five materials (Y_2C, Tb_2C, Dy_2C, Ho_2C) in addition to the previously known M_2N (M = Ca, Sr, Ba) that satisfies all the screening conditions (Table I). We then search literature databases for M_2C, where M is a lanthanide other than Tb, Dy, and Ho, and find a recent article on Gd_2C [13]. Er_2C is mentioned

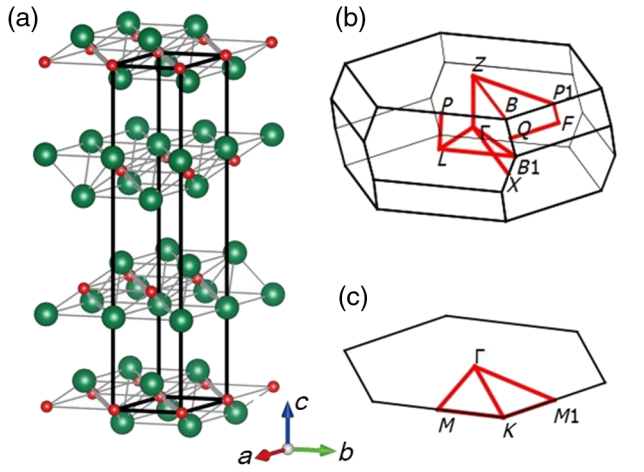

FIG. 2. (a) Crystal structure (anti-$CdCl_2$ structure) of Ca_2N. The large and small spheres denote Ca and N ions, respectively. A conventional unit cell in the hexagonal setting (lattice vectors $\vec{a}$, $\vec{b}$, and $\vec{c}$), containing three primitive rhombohedral cells, is shown by solid lines. (b) BZ for the rhombohedral Bravais lattice and the k path (solid lines) used to plot the band structure in the present paper [22]. In the 2D limit, the BZ in (b) approaches the hexagonally shaped zone in (c).

briefly in Ref. [14] as having the same structure. We include both these materials in our candidate list (Table I). (Because no detailed structural data are available for Er_2C, we assume the structure of Ho_2C.) Initially, we also considered Sc_2C, which met the search conditions, as a candidate, but later rejected it because its entry in the ICSD misrepresented the material: The quoted structure pertains not to pure Sc_2C but to $Sc_2B_{1.1}C_{3.2}$.

A remarkable feature of Table I is that all the materials have the same anti-$CdCl_2$ structure [space group $R\bar{3}m$ (No. 166), with three atoms in the primitive rhombohedral unit cell] shown in Fig. 2(a). Each layer of this structure is made of ions of a single species arranged in a 2D hexagonal close-packed structure, leaving little space inside the layer for electrons to escape into.

Also note that M_2N (M being the divalent cation) has one excess electron per unit cell ($S = 1$) while M'_2C (M' being the trivalent cation) has two excess electrons ($S = 2$). This difference in S results in different band-filling and electronic structures near the Fermi level, as discussed below.

IV. ELECTRONIC STRUCTURE CALCULATIONS

A. Method

We calculate the electronic structures of all the materials listed in Table I and inspect their charge distributions. The calculations are based on density-functional theory using projector-augmented-wave potentials, as implemented in the Vienna *ab initio* simulation package (VASP) [23–26]. Exchange and correlation are treated in the generalized-gradient approximation (GGA) as parametrized by Perdew, Burke, and Ernzerhof [27]. The structures are relaxed until the force acting on each ion becomes less than 0.02 eV/Å. The plane waves used to expand the wave functions are cut off at 800 eV, and integration over the rhombohedral Brillouin zone (BZ) is performed using a $9 \times 9 \times 9$ Γ-centered sampling mesh.

Figure 2(b) shows the BZ for which we present our results, with the k path highlighted by solid lines. The notation follows Ref. [22]. (B_1 is equivalent to B, and X is equivalent to Q by symmetry.) The understanding of band diagrams in the following will be facilitated by noting that the BZ resembles the hexagonal BZ and tends to the hexagonally shaped 2D zone in Fig. 2(c) in the 2D limit (i.e., in the limit of infinite separation between layer units). Thus, the Γ-L-B_1/B-Z (Γ-X/Q-F-P_1-Z) segment may be roughly identified as the Γ-M-K-Γ (Γ-K-M_1-M_1-Γ) segment of the 2D zone. (M and M_1 are not equivalent because the system has only threefold symmetry, not sixfold hexagonal symmetry.)

B. Result for nonmagnetic electride Y_2C

Figure 3(a) presents the calculated results for Ca_2N. The band structures are shown in the left panel while the partial electron densities (PEDs) for states within 0.05 eV of the Fermi level (E_F) are shown in the right panel. (Throughout this paper, the 0 of energy is taken to be the Fermi level.) The conduction band, with its bottom located about 1.7 eV below E_F, can be seen to be a 2D band confined within the gap between the Ca layers, demonstrating that Ca_2N is an electride. Although the band dispersion is free-electron-like, the states near E_F are weakly hybridized with nitrogen p states, as seen in the PED plot.

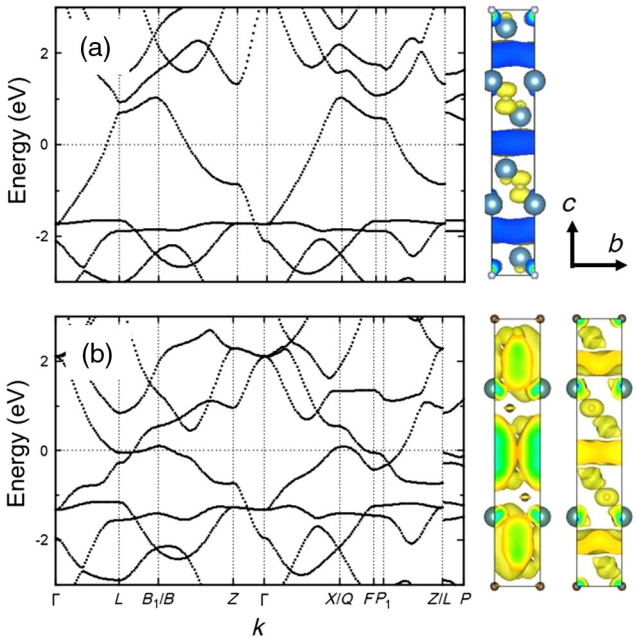

FIG. 3. Calculated energy bands (left) and PED isosurfaces (right) for (a) Ca_2N and (b) Y_2C. The PEDs are calculated for states in the energy range -0.05 eV $< E < 0.05$ eV except for the rightmost PED for Y_2C, which corresponds to an energy range that is 0.3 eV lower, i.e., -0.35 eV $< E < -0.25$ eV. The PEDs are shown for the conventional unit cell [Fig. 2(a)], and the large (small) spheres denote the cations (anions). See also Fig. 4, which presents the variation of the layer-averaged PED in the c direction.

The band structure of Y_2C near E_F [Fig. 3(b)] is similar to that of Ca_2N and shares the same 2D anionic, interlayer character. While the conduction band of Ca_2N is half-filled, it is almost fully occupied in Y_2C and is connected to the higher-energy bands without a gap. The bands overlap slightly near E_F, resulting in a semimetal-like electronic structure. A 2D empty lattice calculation reveals that these bands originate from a single free-electron (parabolic) band folded back into the 2D BZ of Fig. 2(c). The flattening of the bands near E_F makes the conduction-band effective mass of Y_2C heavier than that of Ca_2N. The band filling clearly indicates that there is one excess electron in the unit cell of Ca_2N, in contrast to two excess electrons in the unit cell of Y_2C, justifying our hypothesis (4).

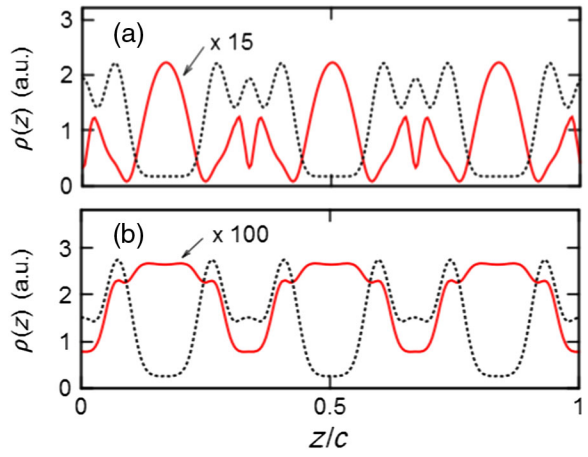

FIG. 4. PED for the energy range from −0.05 to 0.05 eV (solid line) and total valence-electron density (dotted line) for (a) Ca_2N and (b) Y_2C averaged over the ab plane (perpendicular to the c axis) in the conventional unit cell [Fig. 2(a)].

To facilitate understanding of electron localization inside the gap between the cation layers, we average the PED in the layer plane to obtain the 1D partial electron density $\rho_p(z)$. The result is compared for Ca_2N and Y_2C in Fig. 4, where both the PED (thin line) and the total valence-electron density $\rho_v(z)$ (thick line) are plotted. While $\rho_v(z)$ has peaks at ionic layers, $\rho_p(z)$ exhibits a sharp peak at the center of each cation-cation gap and drops rapidly to near 0 as it approaches the cation layers, indicating strong 2D confinement.

Similar localization of conduction electrons in the interlayer gap between cations can also be seen in Y_2C [Fig. 4(b)]. However, the PED is nearly flat across the gap and extends partly into the adjacent Y^{3+} layers, which is consistent with the larger effective mass [the flat dispersion around E_F in Fig. 3(b)].

We examine the variation of the electron confinement with energy and find that the confinement becomes stronger with decreasing energy. The rightmost plot for Y_2C [Fig. 3(b)] shows the PED in the energy range $-0.35\ \text{eV} < E < -0.25\ \text{eV}$. It can be seen that the 2D confinement in this case is stronger than that at E_F, suggesting that greater 2D mobility of the interlayer electrons may be achieved by lowering E_F by hole doping.

The band structures of other nonmagnetic 2D electrides Sr_2N and Ba_2N [10] are shown in Appendix A for the convenience of readers.

C. Results for magnetic electrides

To take account of the strong on-site Coulomb energy and large spin of localized f electrons in lanthanides, we use the spin-polarized GGA + U method to calculate the electronic structure of lanthanide carbides.

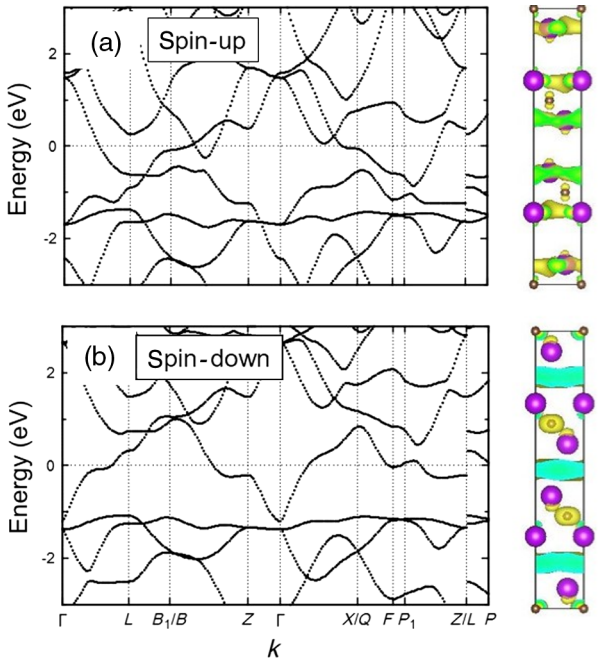

FIG. 5. Calculated energy band and PED isosurface plot for Gd_2C corresponding to each spin channel ($U - J = 6$ eV, $J = 0.7$ eV).

The band structures for the two spin channels of Gd_2C calculated with $U - J = 6$ eV and $J = 0.7$ eV [28] are shown in the left panels of Fig. 5. Aside from the strong spin polarization that lifts the spin-down bands and lowers the spin-up bands, the overall band structures are similar to those of the nonmagnetic 2D electrides (Y_2C, in particular).

There is, however, a striking new feature in the PED (right panels of Fig. 5): The spin-up states near E_F are confined in the cation layer, whereas the spin-down states are confined in the gap between the cation layers to form

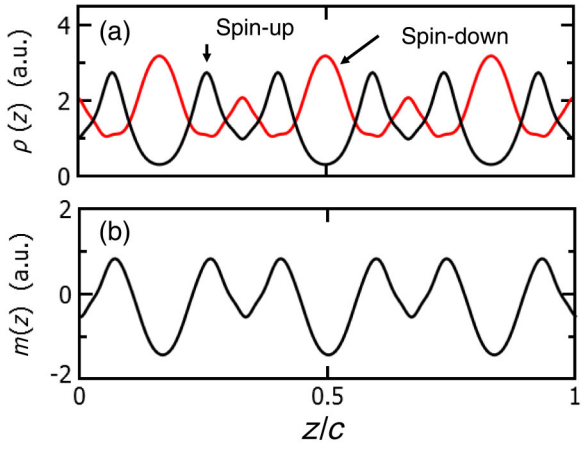

FIG. 6. (a) PED and (b) partial magnetization for Gd_2C within 0.05 eV of E_F averaged over the ab plane ($U - J = 6$ eV, $J = 0.7$ eV).

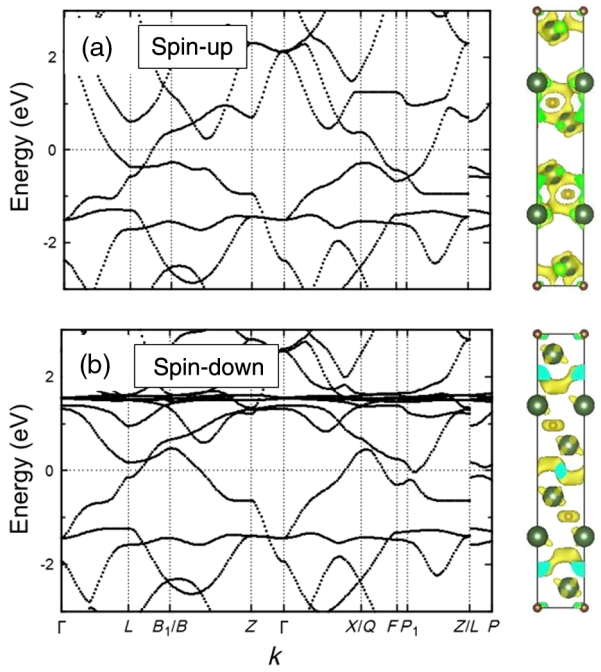

FIG. 7. Calculated energy band and PED isosurface for Er_2C corresponding to each spin channel ($U = 6.7$ eV, $J = 0.7$ eV).

interlayer states similar to those in Ca_2N and Y_2C. This spatial separation of up-spin and down-spin electrons can be seen more clearly in Figs. 6(a) and 6(b), which, respectively, show the layer-averaged PED and partial magnetization. The PEDs for the two spin channels are inversely correlated, producing a striped spatial pattern in the partial magnetization consisting of alternating spin-up and spin-down layers. Note that Fig. 6(b) represents a partial magnetization with electron energy limited to the close vicinity of E_F. The total magnetization (not shown here) is dominated by the strong polarization of the ferromagnetically ordered cation layers. The interlayer anionic electrons are magnetized in the opposite direction,

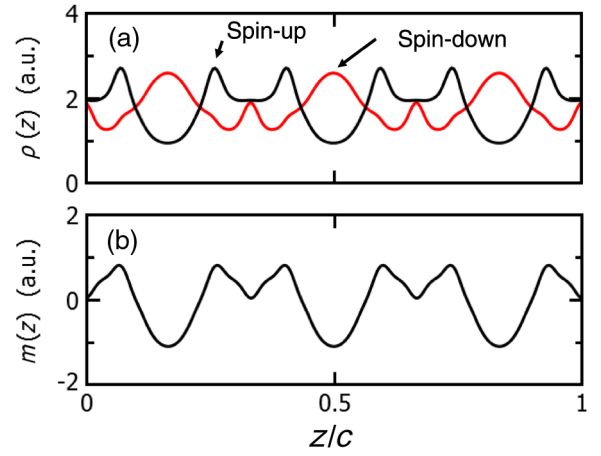

FIG. 8. (a) PED and (b) partial magnetization for Er_2C within 0.05 eV of E_F averaged over the ab plane ($U = 6.7$ eV, $J = 0.7$ eV).

giving a weak ferrimagnetic character to the magnetism of Gd_2C. It was recently reported that Gd_2C is a room-temperature ferromagnet with a Curie temperature of 351 K. The magnetic moment measured per Gd atom is 7.26 [13], which is in reasonably good agreement with our calculation (7.73–7.76, depending on U; see Table I). It remains to be seen how the spatial spin texture of this material is reflected in its magnetization behavior, transport properties, and so forth.

Figure 7 shows the band structure and PED of Er_2C, and Fig. 8 illustrates its layer-averaged PED and partial magnetization. The similarity with Gd_2C is clear, although the 2D confinement is weaker and the PED is not as smooth as that of Gd_2C. This difference may be a result of the smaller spin splitting of Er_2C. For the band structures of magnetic 2D electrides not discussed in this section, see Appendix A.

The above results are obtained for $U - J = 6$ eV and $J = 0.7$ eV. To check their validity, we also carry out calculations for $U - J = 3$ and 9 eV, keeping J fixed at 0.7 eV, and confirm that the results near E_F are essentially the same (Appendix B). The effect of spin-orbit interactions is found to be negligible (Appendix C).

To summarize, all the lanthanide carbides in Table I are 2D magnetic electrides, in which the electrons near E_F in one spin channel float between M_2C layers, while the electrons in the other spin channel reside on these layers.

V. CONCLUSIONS

2D electrides are a novel class of low-dimensional electronic systems, where 2D electrons near E_F exist mainly in the space between ionic layers and are expected to have very high mobility ("2D electron gas in bulk"). These natural "modulation-doped" systems will stimulate research in low-dimensional condensed-matter physics, just as modulation doping has catalyzed a new avenue of semiconductor physics in past decades, leading to the discovery of, for example, integer and fractional quantum Hall effects. We have already initiated the synthesis and transport measurements of some of the materials reported in the present paper [29].

2D electrides are also likely to have an impact on the research in chemistry. In view of the excellent activity of Ru-loaded $C_{12}A_7$ (a zero-dimensional electride) in the synthesis of ammonia from N_2 and H_2 [30], intriguing chemical interactions may take place between these anionic electrons and various external molecules because electrons in 2D electrides can come in direct contact with such molecules.

The Materials Genome Initiative, launched in 2011 by the U.S. government, has revealed to materials researchers the significance of a data-driven approach for accelerating the discovery of new materials [31–35]. The present work, in which six new 2D electrides were identified, is a clear

testimony to the effectiveness of combining large-scale databases and *ab initio* calculations.

ACKNOWLEDGMENTS

T. I. thanks Dr. Susumu Saito for illuminating discussions. This work was supported by the MEXT Elements Strategy Initiative to Form Core Research Center and the JST ACCEL Program.

APPENDIX A: BAND STRUCTURES OF OTHER 2D ELECTRIDES

Figures 9–13 present the band structures of 2D electrides, excepting those discussed already in the main text. Note the close resemblance of Sr_2N (Fig. 9) and Ca_2N [Fig. 3(a)]. The overall band structures of lanthanide dicarbides are similar to each other, and their spin-down interlayer bands [e.g., Fig. 11(b)] have dispersions resembling that of Ba_2N (Fig. 10).

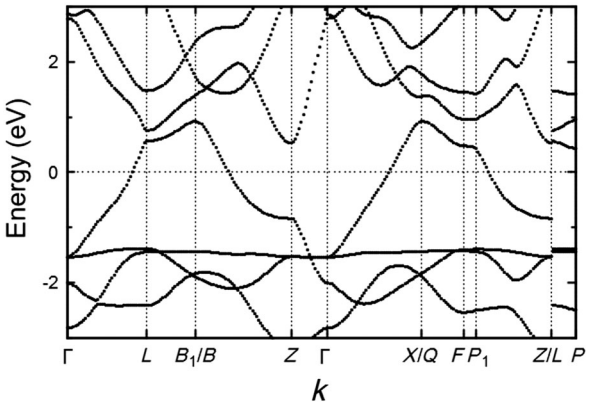

FIG. 9. Calculated band structure of Sr_2N.

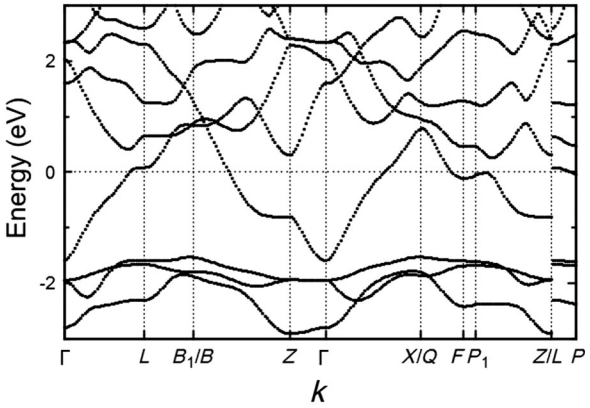

FIG. 10. Calculated band structure of Ba_2N.

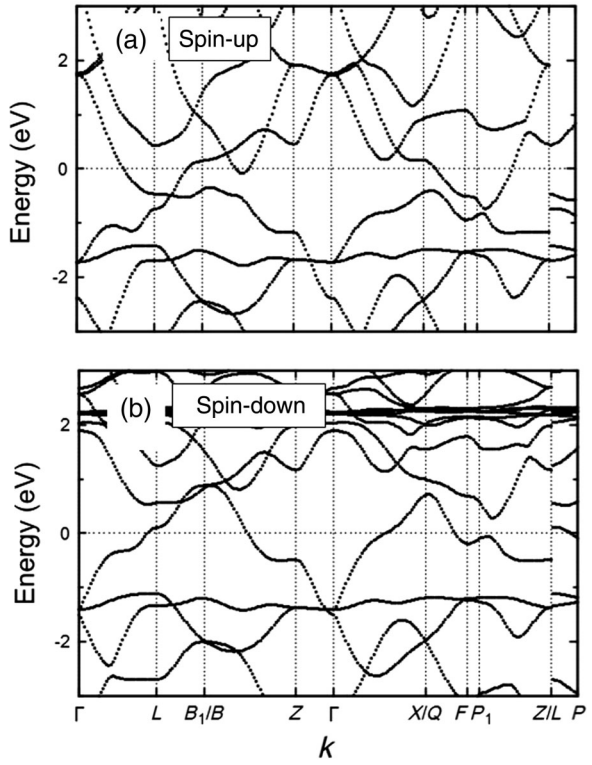

FIG. 11. Calculated band structure of Tb_2C.

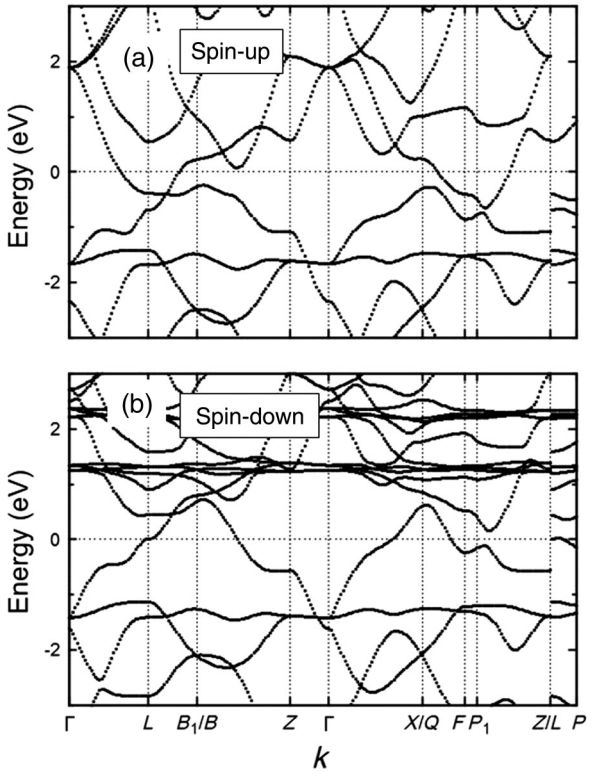

FIG. 12. Calculated band structure of Dy_2C.

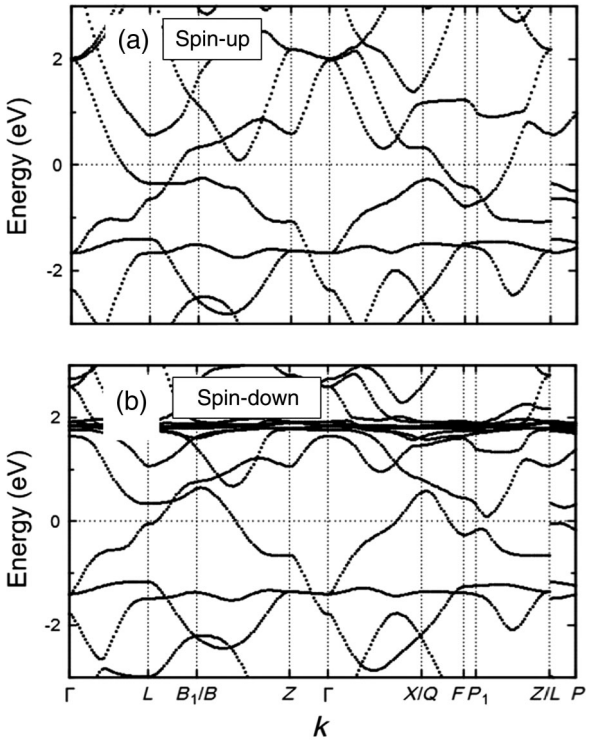

FIG. 13. Calculated band structure of Ho_2C.

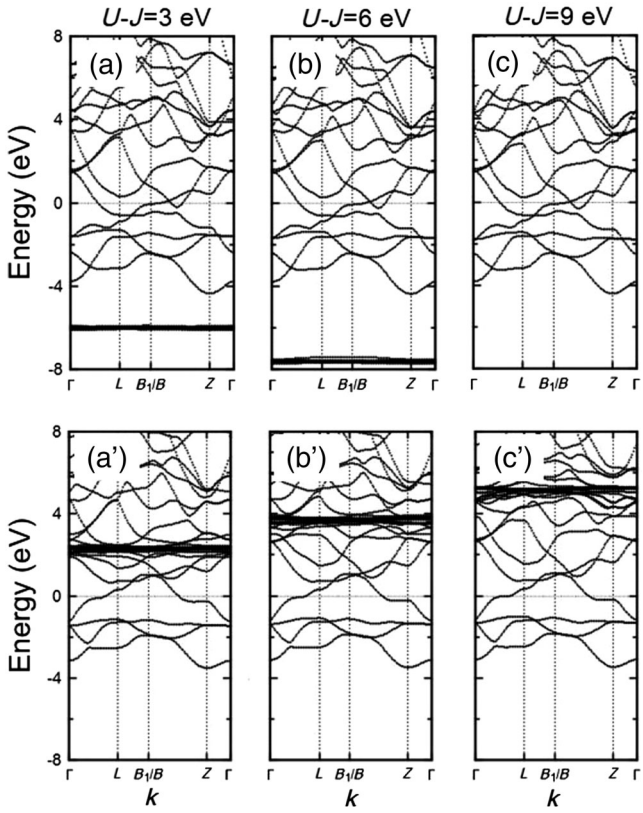

FIG. 14. Band structure for the spin-up electrons of Gd_2C calculated with (a) $U - J = 3$ eV, (b) 6 eV, and (c) 9 eV with J fixed at 0.7 eV. Similar plots for spin-down electrons are shown in (a'), (b'), and (c').

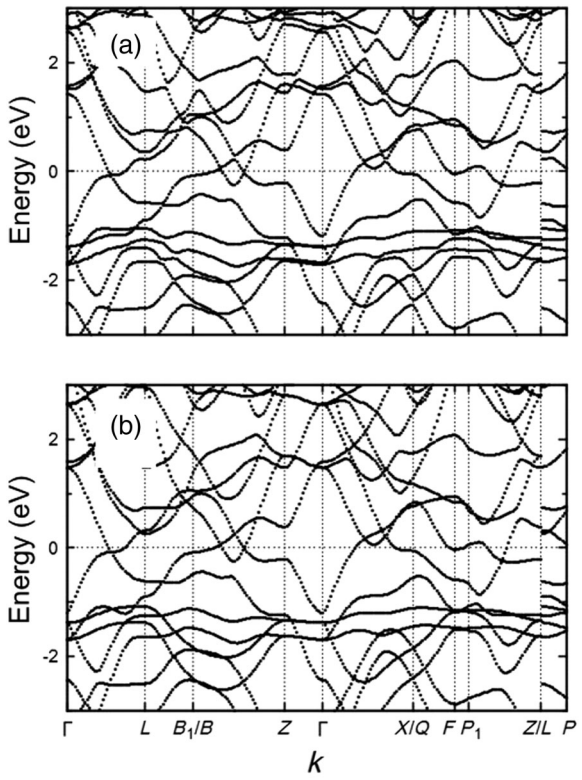

FIG. 15. Band structure of Gd_2C calculated (a) with spin-orbit interaction and (b) without spin-orbit interaction. In (b), both spin channels are plotted simultaneously.

APPENDIX B: COMPARISON BETWEEN CALCULATIONS WITH DIFFERENT U

Figure 14 shows the band structures of Gd_2C obtained with $U - J = 3$, 6, and 9 eV while keeping J fixed at 0.7 eV. With the exception of the flat f bands moving away from E_F as U increases, the bands, particularly those near E_F, are reasonably insensitive to the choice of U. The lattice constants and magnetic moments calculated with different U are in reasonably good agreement, as can be seen in Table I, justifying the use of the GGA + U method in our work.

APPENDIX C: SPIN-ORBIT INTERACTION

Figures 15(a) and 15(b) present the band structures of Gd_2C calculated with and without the spin-orbit interaction, respectively. Note the insensitivity of the interlayer bands near E_F to the interaction. This insensitivity may reflect the small amplitude of the interlayer states at the lanthanide sites.

[1] J. L. Dye, *Electrons as Anions*, Science **301**, 607 (2003).
[2] Some metals (e.g., alkali metals) are also predicted to be electrides under extremely high pressures. See, for example,

C. J. Pickard and R. J. Needs, *Aluminium at Terapascal Pressures*, Nat. Mater. **9**, 624 (2010); M. Gatti, I. V. Tokatly, and A. Rubio, *Sodium: A Charge-Transfer Insulator at High Pressures*, Phys. Rev. Lett. **104**, 216404 (2010); C. J. Pickard and R. J. Needs, *Predicted Pressure-Induced s-Band Ferromagnetism in Alkali Metals*, Phys. Rev. Lett. **107**, 087201 (2011); M.-S. Miao and R. Hoffmann, *High Pressure Electrides: A Predictive Chemical and Physical Theory*, Acc. Chem. Res. **47**, 1311 (2014) and references therein.

[3] J. L. Dye, *Electrides—Ionic Salts with Electrons as the Anions*, Science **247**, 663 (1990).

[4] S.-W. Kim and H. Hosono, *Synthesis and Properties of* $12CaO \cdot 7Al(2)O(3)$ *Electride: Review of Single Crystal and Thin Film Growth*, Philos. Mag. **92**, 2596 (2012).

[5] S. Matsuishi, Y. Toda, M. Miyakawa, K. Hayashi, T. Kamiya, M. Hirano, I. Tanaka, and H. Hosono, *High-Density Electron Anions in a Nanoporous Single Crystal:* $[Ca_{24}Al_{28}O_{64}]^{4+}(4e^-)$, Science **301**, 626 (2003).

[6] D. H. Gregory, A. Bowman, C. F. Baker, and D. P. Weston, *Dicalcium Nitride,* Ca_2N*—a 2D "Excess Electron" Compound; Synthetic Routes and Crystal Chemistry*, J. Mater. Chem. **10**, 1635 (2000).

[7] C. M. Fang, G. A. deWijs, R. A. de Groot, H. T. Hintzen, and G. de With, *Bulk and Surface Electronic Structure of the Layered Sub-Nitrides* Ca_2N *and* Sr_2N, Chem. Mater. **12**, 1847 (2000).

[8] K. Lee, S. W. Kim, Y. Toda, S. Matsuishi, and H. Hosono, *Dicalcium Nitride as a Two-Dimensional Electride with an Anionic Electron Layer*, Nature (London) **494**, 336 (2013).

[9] M. Ujittewaal, G. A. de Wijs, and R. A. de Groot, *Low Work Function of the (1000)* Ca_2N *Surface*, J. Appl. Phys. **96**, 1751 (2004).

[10] A. Walsh and D. O. Scanlon, *Electron Excess in Alkaline Earth Sub-Nitrides: 2D Electron Gas or 3D Electride?*, J. Mater. Chem. C **1**, 3525 (2013).

[11] http://mits.nims.go.jp/index_en.html. MatNavi is a comprehensive materials information platform comprising eight databases plus applications. The crystal structure database is named AtomWork.

[12] http://icsd.fiz-karlsruhe.de/.

[13] Y. Mudryk, D. Paudyal, V. K. Pecharsky, and K. A. Gschneidner, Jr., *Magnetic Properties of* Gd_2C*: Experiment and First Principles Calculations*, J. Appl. Phys. **109**, 07A924 (2011).

[14] M. Atoji, *Neutron-Diffraction Studies of* Tb_2C *and* Dy_2C *in the Temperature Range 4-296 K*, J. Chem. Phys. **75**, 1434 (1981).

[15] C. Baker, M. Barker, and A. Blake, *Calcium Nitride (*Ca_2N*), a Redetermination*, Acta Crystallogr. Sect. E **57**, i6 (2001).

[16] O. Reckeweg and F. J. DiSalvo, *Alkaline Earth Metal Nitride Compounds with the Composition* M_2NX *(*$M = Ca$*, Sr, Ba;* $X = \square$*, H, Cl or Br)*, Solid State Sci. **4**, 575 (2002).

[17] G. V. Vajenine, A. Grzechnik, K. Syassen, I. Loa, M. Hanfland, and A. Simon, *Interplay of Metallic and Ionic Bonding in Layered Subnitrides* AE_2N *(*$AE = Ca$*, Sr, or Ba) Under High Pressure*, Comptes Rendus Chim. **8**, 1897 (2005).

[18] M. Atoji and M. Kikuchi, *Crystal Structures of Cubic and Trigonal Yttrium Hypocarbides; a Dimorphically Interphased Single-Crystal Study*, J. Chem. Phys. **51**, 3863 (1969).

[19] J. P. Maehlen, V. A. Yartys', and B. C. Hauback, *Structural Studies of Deuterides of Yttrium Carbide*, J. Alloys Compd. **351**, 151 (2003).

[20] M. Atoji, *Magnetic and Crystal Structures of the Trigonal* Tb_2C, J. Chem. Phys. **51**, 3872 (1969).

[21] M. Atoji, *Neutron-Diffraction Study of* Ho_2C *at 4-296 K*, J. Chem. Phys. **74**, 1893 (1981).

[22] W. Setyawan and S. Curtarolo, *High-Throughput Electronic Band Structure Calculations: Challenges and Tools*, Comput. Mater. Sci. **49**, 299 (2010).

[23] G. Kresse and J. Furthmüller, *Efficient Iterative Schemes for Ab Initio Total-Energy Calculations Using a Plane-Wave Basis Set*, Phys. Rev. B **54**, 11169 (1996).

[24] G. Kresse and J. Furthmüller, *Efficiency of Ab-Initio Total Energy Calculations for Metals and Semiconductors Using a Plane-Wave Basis Set*, Comput. Mater. Sci. **6**, 15 (1996).

[25] P. E. Blöchl, *Projector Augmented-Wave Method*, Phys. Rev. B **50**, 17953 (1994).

[26] G. Kresse and D. Joubert, *From Ultrasoft Pseudopotentials to the Projector Augmented-Wave Method*, Phys. Rev. B **59**, 1758 (1999).

[27] J. P. Perdew, K. Burke, and M. Ernzerhof, *Generalized Gradient Approximation Made Simple*, Phys. Rev. Lett. **77**, 3865 (1996).

[28] B. N. Harmon, V. P. Antropov, A. I. Liechtenstein, I. V. Solovyev, and V. I. Anisimov, *Calculation of Magneto-optical Properties for* $4f$ *Systems—LSDA Plus Hubbard-U Results*, J. Phys. Chem. Solids **56**, 1521 (1995).

[29] Although the present paper pertains to bulk electrides having 2D electronic structures, it may be interesting to make thin layers of them and study their properties. In a previous paper [8], we successfully exfoliated Ca_2N single crystals by $3M$ tapes [see Fig. 1(b)]. Although single crystals of Y_2C are yet to be synthesized, the samples we have at hand, all polycrystals, consist of thin c-faced platelets. This sample morphology suggests that Y_2C, once synthesized as single crystals, is also exfoliable.

[30] M. Kitano, Y. Inoue, Y. Yamazaki, F. Hayashi, S. Kanbara, S. Matsuishi, T. Yokoyama, S. Kim, M. Hara, and H. Hosono, *Ammonia Synthesis Using a Stable Electride as an Electron Donor and Reversible Hydrogen Store*, Nat. Chem. **4**, 934 (2012).

[31] A. Jain, S. P. Ong, G. Hautier, W. Chen, W. D. Richards, S. Dacek, S. Cholia, D. Gunter, D. Skinner, G. Ceder, and K. A. Persson, *Commentary: The Materials Project: A Materials Genome Approach to Accelerating Materials Innovation*, APL Mater. **1**, 011002 (2013).

[32] S. Lebègue, T. Björkman, M. Klintenberg, R. M. Nieminen, and O. Eriksson, *Two-Dimensional Materials from Data Filtering and Ab Initio Calculations*, Phys. Rev. X **3**, 031002 (2013).

[33] http://aflowlib.org/.

[34] S. Curtarolo, G. L. W. Hart, M. B. Nardelli, N. Mingo, S. Sanvito, and O. Levy, *The High-Throughput Highway to Computational Materials Design*, Nat. Mater. **12**, 191 (2013) and references therein.

[35] https://materialsproject.org/.